Progress In Electromagnetics Research, PIER 99, 289–306, 2009

NUMERICAL ANALYSIS OF APODIZED FIBER BRAGG GRATINGS USING COUPLED MODE THEORY

N.-H. Sun and J.-J. Liau

Department of Electrical Engineering
I-Shou University
Kaohsiung 84001, Taiwan

Y.-W. Kiang

Department of Electrical Engineering and Graduate Institute of Communication Engineering
National Taiwan University
1, Roosevelt Road, Sec. 4, Taipei, Taiwan

S.-C. Lin

Department of Communication Engineering
I-Shou University
Kaohsiung 84001, Taiwan

R.-Y. Ro and J.-S. Chiang

Department of Electrical Engineering
I-Shou University
Kaohsiung 84001, Taiwan

H.-W. Chang

Institute of Electro-optical Engineering and Department of Photonics
National Sun Yat-sen University
Kaohsiung 80424, Taiwan

Abstract—In this paper, the coupled mode theory is used to analyze apodized fiber Bragg gratings (FBGs). Since the profile of gratings varies with the propagation distance, the coupled mode equations (CMEs) of apodized FBGs are solved by the fourth-order Runge-Kutta method (RKM) and piecewise-uniform approach (PUA). We present two discretization techniques of PUA to analyze the apodization profile of gratings. A uniform profile FBG can be expressed as a system

Corresponding author: H.-W. Chang (hchang@faculty.nsysu.edu.tw).

of first-order ordinary differential equations with constant coefficients. The eigenvalue and eigenvector technique as well as the transfer matrix method is applied to analyze apodized FBGs by using PUAs. The transmission and reflection efficiencies calculated by two PUAs are compared with those computed by RKM. The results show that the order of the local truncation error of RKM is h^{-4}, while both PUAs have the same order of the local truncation error of h^{-2}. We find that RKM capable of providing fast-convergent and accurate numerical results is a preferred method in solving apodized FBG problems.

1. INTRODUCTION

Fiber Bragg gratings have been used for spectral filtering, dispersion compensation, wavelength tuning, and sensing in optical communication and optoelectronics [1–3]. Since apodized fiber Bragg gratings (FBGs) have superior filtering performance and high side lobe suppression, apodized FBGs have been widely developed and applied in optical fiber technology Various apodization profiles, such as Gaussian, positive hyperbolic-tangent, quadratic-sine etc. have been studied in literatures [4–7].

A typical 5-mm long FBG has a grating length of up to ten thousand grating periods at the wavelength of 1500 nm. A straight-forward application of the full-wave method [8–13] requires tremendous computer resources in order to sufficiently discretize 3-D (vectorial) field along an FBG fiber. It is possible, for example, to modify the recently published coupled transverse-mode integral-equation (CTMIE) method [11–13] to accurately model the complex reflection and transmission coefficient matrices. Each grating period is first sliced into fifty to one hundred vertical sections to reduce the artificial reflection due to step discretization [13]. Then within each section, four Green's function kernels are constructed from fiber core and as many as cladding modes as needed. As a result, only up to a few grating periods can be computed by CTMIE method. Hence, significant modification of CTMIE is needed to compute apodized FBGs.

Under the principle of the full wave theory, the coupled mode theory (CMT) was developed to analyze "optically large" waveguide structure such as the FBG. CMT captures the main parts of rapidly changing forward and backward propagating phases in an analytic expression and leaves us to deal only with the coupling of slowly varying amplitude envelope functions. These envelope functions satisfy the first-order coupled ordinary differential equation (ODEs) which is

called coupled mode equations. Under CMT, the original full-wave 3D problem is reduced to solving 1-D coupled ODE with boundary conditions on two ends. Consequently, CMT becomes the most common theoretical technique for analyzing uniform FBGs [2]. We believe CMT is also suitable for analyzing the apodized FBG problem.

Recently, we presented a rigorous numerical analysis of the uniform FBG problems with both the eigenvalue and eigenvector technique (EVVT) and RKMs on CMEs with sufficiently high number of core and cladding modes in each fiber direction [14]. RKM was the method of choice for CMEs with z-dependent coefficients. We show that the original inhomogeneous CMEs can be re-casted as constant coefficient ODEs by changing variables. Thus, the ODEs with constant coefficient can be easily and accurately (in numerical sense) solved by EVVT.

Since the structure of apodized FBGs is more complicated than that of uniform FBGs, there are many methods presented to explore the performance of apodized FBGs [14–17]. In this paper, we use CMT to analyze apodized FBGs. Because the profile of gratings depends on the propagation distance, unlike uniform FBGs, the system of the ODEs for apodized FBGs can not be expressed as a system of constant coefficients ODEs by changing variables. This increases the difficulty of analyzing apodized FBGs when compared with analyzing uniform FBGs. The system of the ODEs with z-dependent coefficients can be solved by numerical methods such as RKM [2, 18–20] or Adams-Moulton method (AMM) [21]. Because RKM has benefits of possessing faster convergent rate and being more stable than AMM, in this paper, we choose the fourth-order RKM to solve ODEs with twenty-five fiber modes in each direction. Although RKM was proposed for apodized FBGs in [2], it used only one forward and one backward core modes and ignored core-cladding mode interaction. As far as we know, the detailed algorithmic procedure, accuracy of the solutions and the performance properties of RKM on modeling an apodized FBG have not been discussed in published references. It is the goal of this paper to conduct a thorough error analysis and the convergent rate tests of RKM and two PUA methods on tapered apodized FBGs.

The piecewise-uniform approach (PUA) with transfer matrix method (TMM) is a commonly used numerical technique to simulate apodized grating structures by CMT [4–7]. For traditional PUA, the apodization profile of gratings is discretized into numerous uniform grating sections. To reduce the complexity of the problem, a simplified CMT considers only the coupling between a forward core mode and a backward core mode [4–6]. In this study, the contra-directional coupling between core modes and cladding modes are considered [14].

Although this intuitive PUA has been the chosen method to calculate apodized FBG problems, it needs more numerical work than does RKM. This is because within each uniform FBG section, the transfer matrices still need to be solved by either the modified EVVT method [14] or by RKM. To avoid using modified EVVT we propose the second simplified discrete technique of PUA, where the position of each section is directly substituted into the original CMEs. Since each section of gratings is solved by EVVT the transmission and reflection spectra of apodized FBGs can be obtained by TMM. We compare and analyze the transmission and the reflection efficiencies and their relative error using RKM with those using the two PUAs.

2. THE COUPLE MODE THEORY

2.1. The Gaussian-apodized FBG

The refractive index of the fiber grating is described as follows:

$$n(r,z) = \begin{cases} n_1 + n_1\sigma(z) + n_1\sigma(z)m\cos(2\pi z/\Lambda) & r \le r_1 \\ n_2 & r_1 \le r \le r_2 \\ n_3 & r_2 \le r \end{cases}, \quad (1)$$

where Λ is the grating period n_1, n_2 and n_3 are the refractive indices of the core, cladding and the surrounding region, respectively. $n_1\sigma(z)$ is the dc index change, $n_1\sigma(z)m\cos(2\pi z/\Lambda)$ is the ac index change and m is the fringe visibility of the index change. In this paper, since the FBGs are apodized, $\sigma(z)$ is expressed as a function of a propagation distance. The induced index function $n_1\sigma(z)$ of the Gaussian apodization can be written as:

$$n_1\sigma(z) = n_1\sigma_{dc}\exp\left(-\frac{4\ln(2)z^2}{\mathrm{FWHM}^2}\right) \qquad 0 < z < L, \quad (2)$$

where z is the position of the grating, L is the grating length, and FWHM is the full width at half maximum for induced index function. Fig. 1 shows the induced index change along the fiber axis for Gaussian-apodized structure.

2.2. The Couple Mode Equation

The magnitudes of electromagnetic waves for the ith mode in the fiber can be expressed as

$$\vec{U}_i^{+}(r,\phi,z) = A_i(z)\cdot\vec{\Phi}_i(r,\phi)\cdot\exp(i\beta_i z), \quad (3a)$$

$$\vec{U}_i^{-}(r,\phi,z) = B_i(z)\cdot\vec{\Phi}_i(r,\phi)\cdot\exp(-i\beta_i z), \quad (3b)$$

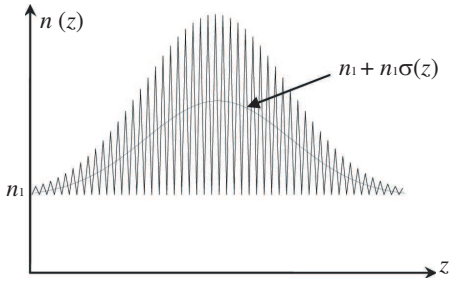

Figure 1. Diagram of the induced index change of Gaussian-apodized grating structure with the fringe visibility m set to one.

where $\vec{U}_i^+(r,\phi,z)$ and $\vec{U}_i^+(r,\phi,z)$ are the magnitudes of forward and backward waves with $A_i(z)$ and $B_i(z)$, the corresponding amplitude functions, $\vec{\Phi}_i(r,\phi)$, the two-dimensional 3-D vector field function, and β_i is the propagation constant of the ith mode.

The couple mode equations of apodized FBGs can be written as

$$\begin{aligned}\frac{dA_0}{dz} &= +i\kappa_0(z)A_0 + i\frac{m}{2}\kappa_0(z)B_0\exp\left(-i2\delta_0 z\right)\\ &\quad +i\sum_{\nu}\frac{m}{2}\kappa_v(z)B_v\exp\left(-i2\delta_v z\right), \qquad (4)\\ \frac{dB_0}{dz} &= -i\kappa_0(z)B_0 - i\frac{m}{2}\kappa_0(z)A_0\exp\left(+i2\delta_0 z\right)\\ &\quad -i\sum_{\nu}\frac{m}{2}\kappa_v A_v(z)\exp\left(+i2\delta_v z\right), \qquad (5)\\ \frac{dA_v}{dz} &= +i\frac{m}{2}\kappa_v(z)B^{co}\exp\left(-i2\delta_v z\right) \quad \text{for } \nu = 1,\cdots,n, \qquad (6)\\ \frac{dB_v}{dz} &= -i\frac{m}{2}\kappa_v(z)A^{co}\exp\left(+i2\delta_v z\right) \quad \text{for } \nu = 1,\cdots,n. \qquad (7)\end{aligned}$$

where $A_0(z)$ is the amplitude for the transverse core mode field traveling to the $+z$ direction, $B_0(z)$ is the amplitude for the transverse core mode field traveling to the $-z$ direction. $A_\nu(z)$ and $B_\nu(z)$ are amplitudes for the νth cladding mode ($v = 1, \ldots, n$). δ is a small-detuning parameter and κ is the coupling coefficient. The parameters δ_0, δ_v, κ_0 and κ_v are defined as follows:

$$\delta_0 = \frac{1}{2}\left(2\beta_0 - \frac{2\pi}{\Lambda}\right), \qquad (8)$$

$$\delta_v = \frac{1}{2}\left(\beta_0 + \beta_v - \frac{2\pi}{\Lambda}\right), \qquad (9)$$

$$\kappa_0(z) = \frac{\omega\varepsilon_0 n_1^2 \sigma(z)}{2} \int_0^{2\pi} d\varphi \int_0^{r_1} r dr \left(|E_r^{co}|^2 + \left|E_\varphi^{co}\right|^2 \right), \quad (10)$$

$$\kappa_v(z) = \frac{\omega\varepsilon_0 n_1^2 \sigma(z)}{2} \int_0^{2\pi} d\phi \int_0^{r_1} r dr \left(E_r^{cl} E_r^{co^*} + E_\phi^{cl} E_\phi^{co^*} \right), \quad (11)$$

where β_0 is the propagation constant of the core mode, β_v is the propagation constant of the vth cladding mode, E_r and E_ϕ are electric fields of transverse components and ω is the angular frequency. Different from the uniform FBGs, $\sigma(z)$ is a function of z for the apodized FBGs, and κ_0 and κ_v are a function of the propagation distance as well. The couple mode equations (CMEs) can be expressed as a matrix form:

$$\frac{d\vec{Y}}{dz} = \frac{d}{dz} \begin{bmatrix} \vec{A} \\ \vec{B} \end{bmatrix} = \begin{bmatrix} \mathbf{U}_{11}(z) & \mathbf{U}_{12}(z) \\ \mathbf{U}_{21}(z) & \mathbf{U}_{22}(z) \end{bmatrix} \cdot \begin{bmatrix} \vec{A} \\ \vec{B} \end{bmatrix} = \mathbf{U}(z) \cdot \vec{Y}, \quad (12)$$

where $\vec{A} = [A_0, \ldots, A_n]^T$ and $\vec{B} = [B_0, \ldots, B_n]^T$ are the amplitude vectors propagating in the forward and backward directions, respectively, and the elements of $\vec{A}$ and $\vec{B}$ are A_v and B_v, $v = 0, \ldots, n$, respectively. The amplitude vector $\vec{Y}$ includes $\vec{A}$ and $\vec{B}$. The matrix $\mathbf{U}$ is a function of the propagation distance z. The elements of sub matrices $\mathbf{U}_{11}$, $\mathbf{U}_{22}$, $\mathbf{U}_{12}$ and $\mathbf{U}_{21}$ are given below

$$\mathbf{U}_{11}(z) = \begin{bmatrix} i\kappa_0(z) & 0 & \cdots & 0 \\ 0 & 0 & \cdots & 0 \\ \vdots & \vdots & \ddots & \vdots \\ 0 & 0 & \cdots & 0 \end{bmatrix} = -\mathbf{U}_{22}(z),$$

$$\mathbf{U}_{12}(z) = \frac{im}{2} \begin{bmatrix} \kappa_0(z)e^{-i2\delta_0 z} & \cdots & \kappa_n(z)e^{-i2\delta_n z} \\ \vdots & 0 & 0 \\ \kappa_n(z)e^{-i2\delta_n z} & 0 & 0 \end{bmatrix}, \quad \text{and} \quad (13)$$

$$\mathbf{U}_{21}(z) = \frac{-im}{2} \begin{bmatrix} \kappa_0(z)e^{i2\delta_0 z} & \cdots & \kappa_n(z)e^{i2\delta_n z} \\ \vdots & 0 & 0 \\ \kappa_n(z)e^{i2\delta_n z} & 0 & 0 \end{bmatrix}.$$

These sub-matrices are functions of propagation distance z makes (12) a system of first-order ODEs with z-dependent coefficients.

3. PIECEWISE-UNIFORM APPROACH

Since the index change $n\sigma(z)$ of the FBGs is a function of z (see Equation (2)), by applying PUA we divide the grating region $0 < z < L$

into M-uniform FBG sections. The position of the i-th section is denoted by $z_i = (i-1) \times L/M$ where $i = 1, \ldots, M$. In this paper, two discrete methods are presented to solve the apodized grating problems and are described as follows:

(1) Note that $\kappa_v(z)$, $\nu = 0, \ldots, n$ in Equation (13) is a function of $n\sigma(z)$ (z) and varies with the propagation distance. The first discretization method, labeled as PUA1, intuitively assumes that the apodization grating consist of multiple uniform gratings. The midpoint approximation is applied to express $n\sigma(z)$ and $\kappa_v(z)$ of each section. An index change of the i-th section is $n\sigma(z_i)$, where $z_i = (i-1) \times L/M$ for $i = 1, \ldots, M$. Although $n\sigma(z_i)$ and $\kappa_v(z_i)$ are constants the coefficients of ODEs in Equation (13) contain exponential terms $\exp(\pm i2\delta_\gamma z)$ for $\nu = 0, \ldots, n$. Therefore, Equation (12) is a system of ODEs with z-dependent coefficients. By changing variables [14], Equation (12) of each section is expressed as a system of ODE with constant coefficients and can be solved by EVVT.

(2) Since the parameters δ_0 and δ_ν are relatively small compared with the propagation constant β_ν the exponential term $\exp(\pm i2\delta_\nu z)$ changes only a few percent over the sub grating section. The second way to discrete gratings, labeled as PUA2, is to directly substitute the position of the i-th section z_i into all of the elements of Equation (13), including $\kappa_v(z_i)$ and $\exp(\pm i2\delta_\gamma z_i)$. Since all elements in Equation (13) are constant we can directly use EVVT to solve Equation (12) without carrying out the additional changing variables step of Reference [14].

Using the above discretization procedures, all elements of $\mathbf{U}$ matrix in Equation (12) become constants, and Equation (12) forms coupled first-order ordinary differential equations with constant coefficients. Both approaches in the i-th section can be solved by EVVT [14]. The amplitude vector function $\vec{Y}_i(z)$ of the section i is expressed as:

$$\begin{aligned}\vec{Y}_i(z) &= \sum_{m=1}^{2n} c_m \cdot \vec{p}_m \cdot e^{\lambda_m z} = \begin{bmatrix} p_{11}e^{\lambda_1 z} & \cdots & p_{1,2n}e^{\lambda_{2n} z} \\ \vdots & \ddots & \vdots \\ p_{2n,1}e^{\lambda_1 z} & \cdots & p_{2n,2n}e^{\lambda_{2n} z} \end{bmatrix} \begin{bmatrix} c_1 \\ \vdots \\ c_{2n} \end{bmatrix} \\ &= \mathbf{Q}_i(z) \cdot \vec{C}_i, \end{aligned} \tag{14}$$

where λ_m and $\vec{p}_m = [\ P_{1,i} \ \cdots \ P_{2n,i}\ ]^T$ are the m-th eigenvalue and its corresponding eigenvector of matrix $\mathbf{U}$ in (12). $\vec{C}_i$ is the unknown eigenfunction coefficient vector which is determined by the boundary conditions. By matching the boundary condition at each

section interface, the amplitudes of modes should be continuous across the interface of sections:

$$\vec{Y}_{i+1}(z_i) = \vec{Y}_i(z_i).$$

The above equation can be written as

$$\mathbf{Q}_{i+1}(z_i) \cdot \vec{C}_{i+1} = \mathbf{Q}_i(z_i) \cdot \vec{C}_i. \tag{15}$$

By using the transfer matrix method, the coefficient vector of the $(i+1)$-th section can be written in terms of the coefficient vector of the i-th section:

$$\vec{C}_{i+1} = \mathbf{Q}_{i+1}(z_i)^{-1} \cdot \mathbf{Q}_i(z_i) \cdot \vec{C}_i = \mathbf{G}_i(z_i) \cdot \vec{C}_i. \tag{16}$$

The amplitudes at $z = L$ can be expressed as

$$\begin{aligned} \vec{Y}(L) &= \mathbf{Q}_M(L) \cdot \vec{C}_M \\ &= \mathbf{Q}_M(L) \cdot \mathbf{G}_{M-1}(z_{M-1}) \cdot \vec{C}_{M-1} \\ &= \mathbf{Q}_M(L) \cdot \mathbf{G}_{M-1}(z_{m-1}) \ldots \mathbf{G}_1(z_1) \cdot \mathbf{Q}_0(0)^{-1} \cdot \vec{Y}(0) \\ &= \mathbf{G}_{\mathrm{PUA}} \cdot \vec{Y}(0), \end{aligned} \tag{17}$$

where $\mathbf{G}_{\mathrm{PUA}}$ is a transform matrix of the stepwise-uniform approach.

4. RUNGE-KUTTA METHOD

Runge-Kutta method (RKM) is the most commonly used numerical method to solve the initial value problem of the ordinary differential equation such as (12). Assume that the grating region $0 < z < L$ is divided by m points. The distance between two adjacent points is $h = L/m$. By applying Runge-Kutta method, the intermediate RK matrices $\mathbf{K}_{1i}$, $\mathbf{K}_{2i}$, $\mathbf{K}_{3i}$ and $\mathbf{K}_{4i}$ inside the i-th fiber section can be expressed as

$$\mathbf{K}_{1i} = h \cdot U(z = L_0 + i \times h), \tag{18}$$

$$\mathbf{K}_{2i} = h \cdot U(z = L_0 + i \times h + h/2) \cdot (\mathbf{I} + \mathbf{K}_{1i}/2), \tag{19}$$

$$\mathbf{K}_{3i} = h \cdot U(z = L_0 + i \times h + h/2) \cdot (\mathbf{I} + \mathbf{K}_{2i}/2), \tag{20}$$

$$\mathbf{K}_{4i} = h \cdot U(z = L_0 + i \times h + h) \cdot (\mathbf{I} + \mathbf{K}_{3i}). \tag{21}$$

The matrix $\mathbf{R}_i$ for this fiber section is written as

$$\mathbf{R}_i = \mathbf{I} + (\mathbf{K}_{1i} + 2\mathbf{K}_{2i} + 2\mathbf{K}_{3i} + \mathbf{K}_{4i})/6, \tag{22}$$

where $\mathbf{I}$ is a unit matrix. The amplitude at point z_{i+1} can be obtained from amplitude at point z_i by using this matrix. We have,

$$\vec{Y}\left((i+1)h\right) = \mathbf{R}_i \cdot \vec{Y}(ih). \tag{23}$$

By repeating Equation (23) for all sub-sections, the amplitudes at $z = L$ can be expressed as

$$\begin{aligned}\vec{Y}(L) = \vec{Y}(Mh) &= \mathbf{R}_{M-1} \cdot \vec{Y}\left((M-1)h\right) \\ &= \mathbf{R}_{M-1} \cdot \mathbf{R}_{M-2} \cdot \vec{Y}\left((M-2)h\right) \\ &= \mathbf{R}_{M-1} \cdot \mathbf{R}_{M-2} \cdot \ldots \cdot \mathbf{R}_i \cdot \mathbf{R}_{i-1} \ldots \mathbf{R}_0 \cdot \vec{Y}(0) \\ &= \mathbf{G}_{\mathrm{RKM}} \cdot \vec{Y}(0). \end{aligned} \tag{24}$$

where matrix $\mathbf{G}_{\mathrm{RKM}}$ is a transfer matrix of Runge-Kutta method.

To calculate transmission and reflection coefficients, (17) and (24) can be written as

$$\begin{bmatrix} \vec{A}(L) \\ \vec{B}(L) \end{bmatrix} = \begin{bmatrix} \mathbf{G}_{11} & \mathbf{G}_{21} \\ \mathbf{G}_{21} & \mathbf{G}_{22} \end{bmatrix} \begin{bmatrix} \vec{A}(0) \\ \vec{B}(0) \end{bmatrix}, \tag{25}$$

where $\mathbf{G}_{11}$, $\mathbf{G}_{12}$, $\mathbf{G}_{21}$ and $\mathbf{G}_{22}$ are submatrices of either $\mathbf{G}_{\mathrm{PUA}}$ in (17) or $\mathbf{G}_{\mathrm{RKM}}$ in (24). Assume that core mode is incident from $z = 0$, and no reflection wave exists at $z = L$. $\vec{A}(L)$, the transmission amplitude vector at $z = L$ and $\vec{B}(0)$, the reflection amplitude vector at $z = 0$ can be expressed as

$$\vec{B}(0) = \mathbf{G}_{22}^{-1} \cdot \vec{B}(L) - \mathbf{G}_{22}^{-1} \cdot \mathbf{G}_{21} \cdot \vec{A}(0), \tag{26}$$

$$\vec{A}(L) = \left(\mathbf{G}_{11} - \mathbf{G}_{12} \cdot \mathbf{G}_{22}^{-1} \cdot \mathbf{G}_{21}\right) \cdot \vec{A}(0) + \mathbf{G}_{12} \cdot \mathbf{G}_{22}^{-1} \cdot \vec{B}(L). \tag{27}$$

We can obtain the transmission and reflection efficiencies of the core mode:

$$T = \frac{|A_0(L)|^2}{|A_0(0)|^2} = |A_0(L)|^2, \quad R = \frac{|B_0(0)|^2}{|A_0(0)|^2} = |B_0(0)|^2. \tag{28}$$

5. RESULTS AND DISCUSSION

A step index fiber is considered in this paper. The FBG is assumed to be made of a single mode fiber. For fiber structure, the radius of core and cladding are $r_1 = 2.5\,\mu\mathrm{m}$ and $r_2 = 62.5\,\mu\mathrm{m}$, respectively. The corresponding refractive indices are n_1=1.458 and $n_2 = 1.45$. Consider a Gaussian apodization profile of gratings with the grating period of $\Lambda = 0.53\,\mu\mathrm{m}$. The maximum value of induced-index change $n_1\sigma(z)$ is 2.8×10^{-3}, the FWHM = 4 mm, the fringe visibility of the index change in Equation (1) is 1, and the total length of the FBG is $L = 4\,\mathrm{mm}$ [1, 2].

We choose PUA1 to calculate the spectrum of apodized FBGs. Figs. 2(a) and 2(b) show the transmission spectrum and reflection

spectrum of Gaussian-apodized FBGs calculated by PUA1 (solid line) and RKM (dashed line). One core mode and twenty-four cladding modes are calculated in this analysis. The grating region is divided by 1000 sections by PUA1, while the step number of RKM is 1000. Notably, the transmission and reflection spectra of apodized FBGs are not symmetric at the resonant region. The 3 dB resonant region is from 1539.92 nm to 1541.70 nm, and the 3 dB bandwidth is 1.78 nm. For the reflection spectrum, there are high sidelobes at short wavelength of the resonant region, while very low sidelobe is at the long wavelength side. The sidelobe suppression at the long wavelength side is 95.36% at the wavelength of 1542.02 nm. The first sidelobe at the short wavelength side occurs at the wavelength of 1539.87 nm with the reflection efficiency of 0.993. The high sidelobes at the short wavelength are caused by the dc index change of Gaussian apodization [1]. Note that the contra-directional cladding mode coupling occurs at the wavelength less than 1539 nm in Fig. 2(a) because both the transmitted and reflected powers in Figs. 2(a) and 2(b) are decreased.

Since the apodized FBG problem is difficult to calculate, for the sake of simplicity, many published results considered only the coupling between a forward core mode and a backward core mode [4–6]. In this paper we consider a total of 25 modes (1 core mode and 24 cladding modes) in CMEs (4)–(7). The comparison of the transmission and reflection spectra between 1 mode and 25 modes are displayed in Figs. 3(a) and 3(b), respectively, by using RKM with 1000 steps. We find that both spectra computed from considering 1 mode slightly shift 0.03 nm toward the short wavelength when compared with those from 25 modes. The spectra in Figs. 3(a) and 3(b) in the long wavelength side are similar, whereas the transmission spectra are very different in Fig. 3(a) due to the contra-directional cladding mode coupling for the wavelength less than 1539 nm. It is because the effective indices of cladding modes increase with decreased wavelengths. When the forward core mode is coupled with the backward cladding modes, the transmission efficiencies decrease. On the other hand, the coupling power does not transfer the forward power to backward core mode. Therefore, the reflection efficiency of the core mode remains low. Figs. 4(a) and 4(b) show that a significant error of the transmission spectrum occurs without considering cladding mode coupling.

The differences of transmissivity and reflectivity calculated by PUA1 and RKM are shown in Figs. 4(a) and 4(b), respectively. The relative difference at resonance is less than those off resonance. The differences in the resonant region are less than 10^{-9} and 10^{-8} for the transmission and reflection efficiencies, respectively. The maximum differences of transmissivity and reflectivity in Fig. 4 occur at the

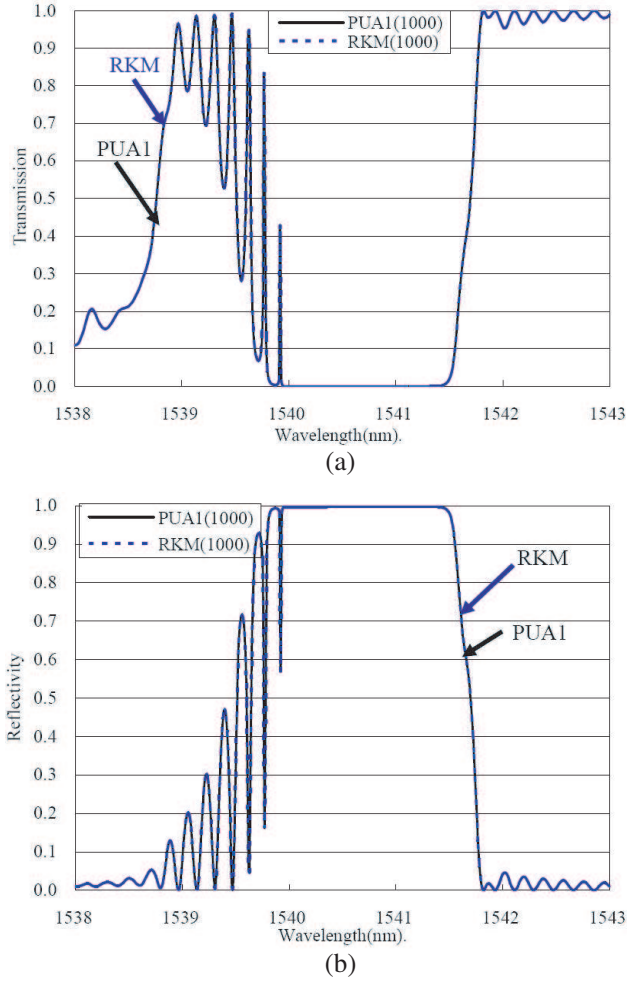

Figure 2. (a) The transmission spectrum of Gaussian-apodized gratings, (b) the reflection spectrum of Gaussian-apodized gratings. The solid line is calculated by PUA, the dash line is calculated by RKM.

wavelength of 1539.92 nm, which locates at the edge of the resonant region (the short wavelength side). Both differences of transmission and reflection are less than 6.5×10^{-5}. It is apparently that the numerical errors of transmission and reflection are mainly caused by the coefficients of A_0 and B_0 in (12), $\mp(m/2)\kappa_0(z)\exp(\pm i2\delta_0 z)$. Since the exponential term $\exp(\pm i2\delta_0 z)$ varies faster than $\kappa_0(z)$, it dominates

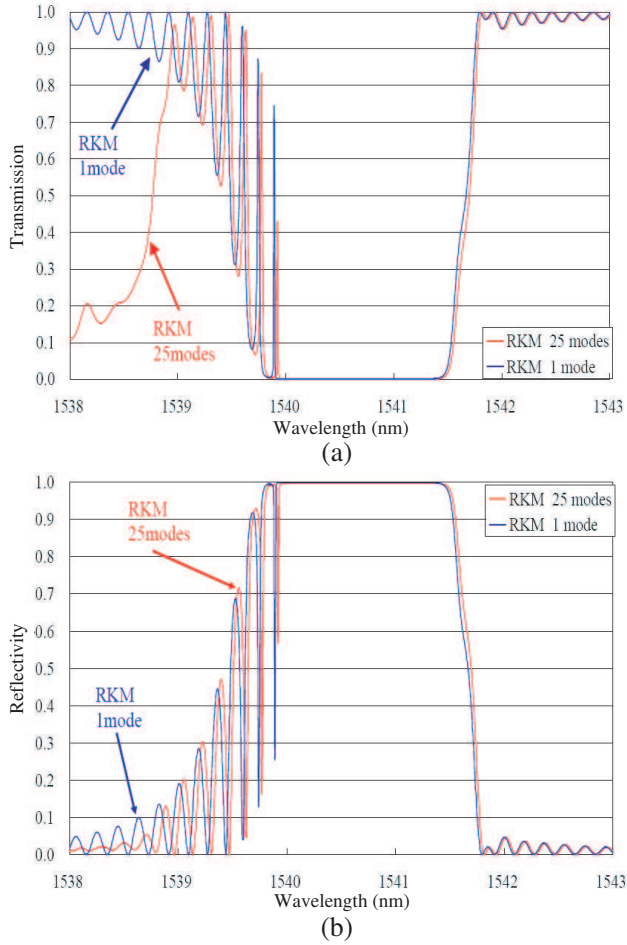

Figure 3. (a) The transmission spectrum and (b) the reflection spectrum of Gaussian-apodized gratings calculated by RKM with the fundamental core mode and with a total of 25 modes (one fundamental mode and 24 cladding modes).

the numerical error in the calculation. At resonance, the parameter of the core mode δ_0 in (8) approaches zero. The coefficients of A_0 and B_0 in (12) are near constants. Therefore, A_0 and B_0 can be calculated with small numerical error.

Since all calculated transmission and reflection powers approach to those by RKM with large step numbers, high step RKM can provide more accurate solutions than the other methods. We choose the transmissivity and reflectivity obtained by RKM for 20000 steps as the

reference results at 1539.92 nm. This point is chosen as the reference because it is accurate to 12 decimal places. The wavelength is chosen because of the maximum error occurred in Fig. 4. Figs. 5(a) and 5(b) show the errors of transmission and reflectivity calculated by PUA1, PUA2 and RKM as a function of the number of divided regions for PUA and step number for RKM. The errors are caused by insufficient discretization in both the PUA and RKM methods. They are defined as the difference between calculated values and the reference results

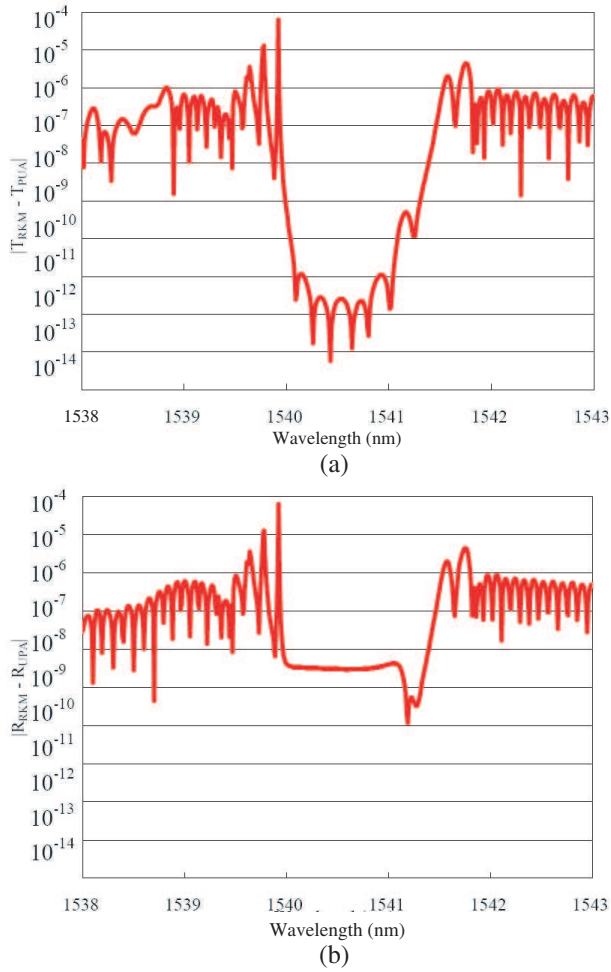

Figure 4. (a) The difference of the transmission efficiencies between the PUA1 and RKM, (b) the difference of the reflection efficiencies between the PUA1 and RKM.

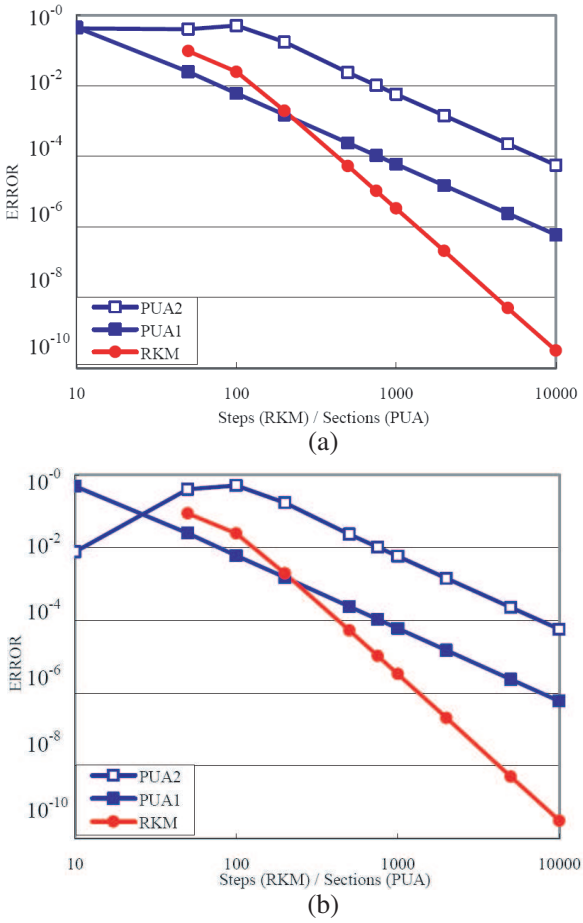

Figure 5. (a) The error of transmissivity by RKM, PUA1 and PUA2 as a function of step numbers at wavelength of 1539.92 nm, (b) the error of reflectivity by RKM, PUA1 and PUA2 as a function of step numbers at wavelength of 1539.92 nm.

(RKM with 20000 steps).

As shown in Fig. 5, the truncation error of transmissivity and reflectivity for PUA1, PUA2 and RKM decrease with increased section number or step number. Compare Figs. 5(a) with Fig. 5(b). The calculated errors of PUA1, PUA2 and RKM for the transmission efficiency (Fig. 5(a)) and the reflection efficiency (Fig. 5(b)) are very similar. For RKM, when the step size h in Figs. 5(a) and 5(b) is decreased by 10^{-1}, the local truncation error decreases to 10^{-4} times. That indicates the order of the local truncation error is h^{-4}. The

rate of convergence for RKM (or the local truncation error of RKM) can also be denoted as $O(h^{-4})$. The truncation error is the same as theoretical results of the fourth-order RKM. On the other hand, both PUA1 and PUA2 in Figs. 5(a) and 5(b) have similar decreased slopes and represent the same local truncation error of h^{-2} when the step number is greater than 100. It is noted that the error of PUA2 is about 100 times of the error of PUA1. At the step number of 10000, for example, the error of reflectivity of PUA2 is 5.66×10^{-5}, while the error of PUA1 is 5.98×10^{-7}.

Table 1 lists the propagation constants β_ν and FBG parameters κ_ν, δ_ν of the core mode and the first nine cladding modes. We can find that δ_ν is about two thousandth of κ_ν for $\nu = 0$. Although PUA2 is an easy and simple method to discretize the apodized FBG, the numerical error is acceptable and decreasing as we increase the steps. That means for PUA2, the constant approximation of the exponential terms $\exp(\pm i2\delta_\nu z)$ in (12) does not produce significant numerical errors. It is because the maximum value of $2\delta_\nu L/2\pi$ in Table 1 is less than fifteen. Since $\exp(\pm i2\delta_\nu z)$ fluctuates at most fifteen cycles over the entire FBG length ($L = 4\,\text{mm}$), as shown in Fig. 5, a number of 100 discrete sections of PUA2 are sufficient to obtain reasonable numerical results (about 7 points per wavelength). At the step number of 100, the error of reflectivity of PUA1 and PUA2 are 5.98×10^{-5} and 5.71×10^{-3}, respectively. In general, PUA2 requires fewer numerical tasks than PUA1. It provides acceptable numerical solutions in most apodized FBG design projects. We also find that RKM has larger error than PUA1 when the step size is less than 100 which is quite inadequate to

Table 1. The propagation constant β_v and FBG parameters κ_ν, δ_ν at $\lambda = 1539.92\,\text{nm}$. The unit is given in MKS system (M^{-1}).

ν	mode	$\beta_v \times 10^{-6}$	$\kappa_v \times 10^{-6}$	$\delta_\nu \times 10^{-3}$
0	$HE_{1\text{-}1}$	5.92449	6.474421	−3.0479
1	$HE_{1\text{-}2}$	5.91608	0.299193	−7.2513
2	$EH_{1\text{-}1}$	5.91573	0.542415	−7.4276
3	$HE_{1\text{-}3}$	5.91536	0.741188	−7.6090
4	$EH_{1\text{-}2}$	5.91479	0.896998	−7.0610
5	$HE_{1\text{-}4}$	5.91416	1.014942	−8.2091
6	$EH_{1\text{-}3}$	5.91339	1.101888	−8.5966
7	$HE_{1\text{-}5}$	5.91249	1.164313	−9.0451
8	$EH_{1\text{-}4}$	5.91158	1.207436	−9.4995
9	$HE_{1\text{-}6}$	5.91036	1.235133	−10.1121

sample the sinusoidal amplitude fluctuation due to κ_ν term in CMT Equations (4)–(7). The RKM and PUA1 have similar truncation error at the step number/section number of 200.

6. CONCLUSIONS

In this paper, the couple mode theory is applied to analyze the Gaussian-apodized FBGs. Runge-Kutta method and the piecewise-uniform approach are used to calculate the transmission and reflection efficiencies of Gaussian-apodized FBGs. Two discretization methods, PUA1 and PUA2, are proposed to discretize the apodization profile of gratings.

We present the transmission and reflection spectra of Gaussian-apodized FBGs and compare the difference of the results calculated by PUA and RKM. Since the results by PUA1 and PUA2 approach those by RKM with 10000 steps, the results by RKM of 10000 steps are chosen as the reference number. The calculated results show that the order of the local truncation error for RKM is h^{-4}. The RKM produces accurate results with fast convergent rate. The numerical procedure for RKM can be easily developed to analyze apodized FBGs. Therefore, RKM is a preferred method in solving apodized FBG problems when high numerical accuracy is required. On the other hand, the convergent rates of PUA1 and PUA2 are both $O(h^{-2})$. At the section number of 100 and beyond, the errors of PUA2 for the transmission and reflection efficiencies are 100 times larger than those of PUA1 at the wavelength of 1539.92 nm. Nevertheless, PUA2 is a simpler method than PUA1, and can provide acceptable numerical results in most cases.

ACKNOWLEDGMENT

The authors are grateful to the support of the National Science Council of the Republic of China under the contracts NSC97-972221-E-110016, NSC93-2215-E-214-03 and NSC96-2221-E-214-023-MY3. This work is also supported by the Ministry of Education, Taiwan, under the Aim-for-the-Top University Plan.

REFERENCES

1. Erdogan, T., "Fiber grating spectra," *J. Lightwave Technol.*, Vol. 15, 1277–1294, 1997.
2. Erdogan, T., "Cladding-mode resonances in short- and long-period fiber grating filters," *J. Opt. Soc. Am. A*, Vol. 14, 1760–1773, 1997.

3. He, M., J. Jiang, J. Han, and T. Liu, "An experiment research on extend range of Based on fiber Bragg grating demodulation based on CWDM," *Progress In Electromagnetics Research Letters*, Vol. 6, 115–121, 2009.
4. Ennser, K., M. N. Zervas, and R. I. Laming, "Optimization of apodized linearly chirped fiber gratings for optical communications," *IEEE J. Quantum Electron.*, Vol. 34, 770–778, 1998.
5. Lima, M. J. N., A. L. J. Teixeira, and J. R. F. Da Rocha, "Optimization of apodized fiber grating filters for WDM systems," *Proc. of IEEE LEOS Annual Meeting, ThZ2*, 876–877, San Francisco, USA, 1999.
6. Rebola, J. L. and A. V. T. Cartaxo, "Performance optimization of gaussian apodized fiber Bragg grating filter in WDM systems," *IEEE Journal of Lightwave Technology*, Vol. 20, 1537–1544, 2002.
7. Moghimi, M. J., H. Ghafoori-Fard, and A. Rostami, "Analysis and design of all-optical switching in apodized and chirped Bragg gratings," *Progress In Electromagnetics Research B*, Vol. 8, 87–102, 2008.
8. Sha, W. E. I., X.-L. Wu, Z.-X. Huang, and M.-S. Chen, "Waveguide simulation using the high-order symplectic finite-difference time-domain scheme," *Progress In Electromagnetics Research B*, Vol. 13, 237–256, 2009.
9. Khajehpour, A. and S. A. Mirtaheri, "Analysis of pyramid EM wave absorber by FDTD method and comparing with capacitance and homogenization methods," *Progress In Electromagnetics Research Letters*, Vol. 3, 123–131, 2008.
10. Hattori, H. T., "Fractal-like square lattices of air holes," *Progress In Electromagnetics Research Letters*, Vol. 4, 9–16, 2008.
11. Chang, H.-W. and M.-H. Sheng, "Field analysis of dielectric waveguide devices based on coupled transverse-mode integral equation — Mathematical and numerical formulations," *Progress In Electromagnetics Research*, PIER 78, 329–347, 2008.
12. Chang, H.-W. and M.-H. Sheng, "Errata for the paper entitled 'dielectric waveguide devices based on coupled transverse-mode integral equation — Mathematical and numerical formulations'," *Progress In Electromagnetics Research C*, Vol. 8, 195–197, 2009.
13. Chang, H.-W., Y.-H. Wu, S.-M. Lu, W.-C. Cheng, and M.-H. Sheng, "Field analysis of dielectric waveguide devices based on coupled transverse-mode integral equation — Numerical investigation," *Progress In Electromagnetics Research*, PIER 97, 159–176, 2009.

14. Liau, J.-J., N.-H. Sun, S.-C. Lin, R.-Y. Ro, J.-S. Chiang, C.-L. Pan, and H.-W. Chang, "A new look at numerical analysis of uniform fiber Bragg gratings using coupled mode theory," *Progress In Electromagnetics Research*, PIER 93, 385–401, 2009.
15. Feced, R., M. N. Zervas, and M. A. Muriel, "An efficient inverse scattering algorithm for the design of nonuniform fiber Bragg gratings," *IEEE J. Quantum Electron.*, Vol. 35, 1105–1115, 1999.
16. Rostami, A. and A. Yazdanpanah-Goharrizi, "A new method for classification and identification of complex fiber Bragg grating using the genetic algorithm," *Progress In Electromagnetics Research*, PIER 75, 1105–1115, 2007.
17. Prokopovich, D. V., A. V. Popov, and A. V. Vinogradov, "Analytical and numerical aspects of Bragg fiber design," *Progress In Electromagnetics Research B*, Vol. 6, 361–379, 2008.
18. Watanabe, K., "Fast converging and widely applicable formulation of the differential theory for anisotropic gratings," *Progress In Electromagnetics Research*, PIER 48, 279–299, 2004.
19. Rojas, J. A. M., J. Alpuente, P. López-Espí, and P. García, "Accurate model of electromagnetic wave propagation unidimensional photonic crystals with defects," *Journal of Electromagnetic Waves and Applications*, Vol. 21, No. 8, 1037–1051, 2007.
20. Molinet, F. A., "Plane wave diffraction by a strongly elongated object illuminated in the paraxial direction," *Progress In Electromagnetics Research B*, Vol. 6, 135–151, 2008.
21. Chang, K. C., V. Shah, and T. Tamir, "Scattering and guiding of waves by dielectric gratings with arbitrary profiles," *J. Opt. Soc. Amer.*, Vol. 70, 804–813, 1980.